Journal of
Marine Science and Engineering

MDPI

Article

An Econometric Analysis of Sea Surface Temperatures, Sea Ice Concentrations and Ocean Surface Current Velocities

Alok Bhargava [1,*] and Juan A. Echenique [2]

[1] School of Public Policy, University of Maryland, College Park, MD 20742, USA
[2] Grossman School of Medicine, New York University, New York, NY 10016, USA
* Correspondence: bhargava@umd.edu

Abstract: This paper analyzed quarterly longitudinal data for 64,800 1 × 1 degree grids during 2000–2019 on sea surface temperatures, sea ice concentrations, and ocean surface current zonal and meridional velocities in the Northern and Southern hemispheres. The methodological framework addressed the processing of remote sensing signals, interdependence between sea surface temperatures and sea ice concentrations, and combining zonal and meridional velocities as the eddy kinetic energy. Dynamic and static random effects models were estimated by maximum likelihood and stepwise methods, respectively, taking into account the unobserved heterogeneity across grids. The main findings were that quarterly sea surface temperatures increased steadily in the Northern hemisphere, whereas cyclical patterns were apparent in Southern hemisphere; sea ice concentrations declined in both hemispheres. Second, sea surface temperatures were estimated with large negative coefficients in the models for sea ice concentrations for the hemispheres; previous sea ice concentrations were negatively associated with sea surface temperatures, indicating feedback loops. Third, sea surface temperatures were positively and significantly associated with eddy kinetic energy in Northern hemisphere. Overall, the results indicated the importance of reducing sea surface temperatures via reductions in greenhouse gas emissions and the dumping of pollutants into oceans for maintaining sea ice concentrations and enhancing global sustainability.

Keywords: climate change; sea surface temperatures; sea ice concentrations; ocean surface current velocities; maximum likelihood estimation; mitigation policies; remote sensing data

check for updates

Citation: Bhargava, A.; Echenique, J.A. An Econometric Analysis of Sea Surface Temperatures, Sea Ice Concentrations and Ocean Surface Current Velocities. *J. Mar. Sci. Eng.* **2022**, *10*, 1854. https://doi.org/10.3390/jmse10121854

Academic Editors: Mark D. Orzech, Jie Yu and Michael H. Meylan

Received: 18 October 2022
Accepted: 25 November 2022
Published: 1 December 2022

1. Introduction

While the role of atmospheric concentrations of greenhouse gases such as carbon dioxide, methane and nitrous oxide for increasing the ambient temperatures has long been recognized [1,2], agreements between countries for limiting emissions require complex negotiations [3] due to the need for meeting energy demand and for maintaining agricultural, industrial, and economic activities. It is therefore not surprising that, despite pledges from governments, atmospheric concentrations of greenhouse gases have steadily increased in the past decades [4]. Moreover, the role of oceans and cryosphere for maintaining the Earth's radiation budget deserves greater emphasis [5]; warming of oceans can reduce sea thicknesses and concentrations and set off feedback effects thereby accelerating global warming [6]. The formulation of evidence-based climate policies is facilitated by employing broad analytical frameworks and conducting analyses of longitudinal data spanning several years for the hemispheres [7].

Further, while a high proportion of carbon dioxide is ultimately absorbed by the oceans, thereby lowering pH levels [8], industrial and agricultural waste and plastics flow into the oceans, thereby increasing eutrophication of coastal waters [9–11] and altering sea water composition, including freezing points [12,13]. Such factors are likely to increase sea surface temperatures and reduce the concentrations of sea ice that is often connected with polar ice sheets [14]; glacier and ice sheet concentrations are adversely affected by aerosols

from pollution [15]. In addition, over a long timeframe, zonal and meridional velocities of ocean surface currents may be affected by the increases in sea surface temperatures [16]. For example, small velocity changes in the Atlantic Meridional Overturning Circulation [17], which takes over a millennium for completing a cycle, could have differential effects for warming patterns of the continents. While remote sensing longitudinal data on sea surface temperatures, sea ice concentrations, and zonal and meridional ocean surface current velocities are available, respectively, for 0.05 × 0.05, 0.01 × 0.01 and 0.33 × 0.33-degree grids [18–20], the dynamic inter-relationships between these indicators have apparently not been analyzed. Analyses of a merged data set for 1 × 1-degree grids during 2000–2019 using the appropriate statistical and econometric methods can provide insights for the formulation of evidence-based climate policies.

From a measurement standpoint, processing thermal infrared radiance from orbiting satellites for constructing sea surface temperatures is complex and entails combining signals from advanced very high-resolution radiometers and along-track scanning radiometers that have different resolutions [19]. Subsequently, the noise in signals due to clouds and other factors is reduced via interpolation and filtering techniques [21,22]. Similarly, the assessment of sea ice thicknesses and concentrations via satellites requires approximations for "freeboard" and sea surface levels, as well as for the densities of snow and sea water [23,24]. Furthermore, zonal and meridional velocities of ocean surface currents are estimated from satellite signals based on geostrophy, Ekman dynamics, and thermal winds [25]. However, the underlying nonlinear interactions between factors such as wind, waves, turbulence, tides, baroclinic instabilities, and barotropic pressure gradients are difficult to capture adequately [26]. While drifting satellite-tracked instruments can provide insights into ocean surface currents [27,28], thermodynamic influences of deep-ocean currents require in situ measurements covering vast areas that may be infeasible. Despite the measurement difficulties, it is important to investigate the effects of sea surface temperatures for zonal and meridional velocities of ocean surface currents [29]. It may be useful to combine the two velocities as the eddy kinetic energy since the latter may better reflect sea water movements [30,31].

Lastly, modelling the dynamic interrelationships between the sea surface temperatures, sea ice concentrations, and ocean surface current velocities would benefit from analyzing quarterly longitudinal data since these indicators critically depend on seasons in the hemispheres. Moreover, sea surface temperatures are likely to increase due to the absorption of heat and greenhouse gases from land; industrial and agricultural pollutants can reduce sea ice concentrations and affect ocean surface current velocities. In addition, reduced sea ice concentrations in the previous quarter can increase sea surface temperatures in subsequent quarters. Although the existence of feedback effects has been postulated in the climate literature, investigating their magnitudes entails the estimation of empirical models using quarterly data for a common grid size. The use of 1 × 1 degree grids is appealing partly because of the interpolations employed in processing the remote sensing signals [32]. The formulation of evidence-based policies will benefit from utilizing the parameters estimated from longitudinal data analyses.

The structure of this paper is as follows: Section 2 describes the processing of remote sensing data for the sea surface temperatures, sea ice concentrations, and zonal and meridional velocities of ocean surface currents. The analytical framework is outlined in Section 3, and the empirical models are presented, taking into account the measurement aspects. Section 3.2 discusses statistical issues arising in the estimation of the empirical models. The descriptive statistics and *t*-tests for changes in climate indicators during 2000–2019 are presented in Section 4. The results from empirical models for the sea surface temperatures, sea ice concentrations, and ocean surface current velocities and eddy kinetic energy are presented in Sections 5–7, respectively. The conclusions and the need for further research are discussed in Section 8.

2. Materials and Methods

The Remote Sensing Data Sets

The remote sensing data for sea surface temperatures were processed for 0.05 × 0.05-degree grids using several mathematical techniques ("Level 4 analyses") [19]. Initially, thermal infrared radiance measurements were collected via two series of sensors from orbiting satellites: 11 advanced very high-resolution radiometers and three along-track scanning radiometers. Because "skin" sea surface temperatures are sensitive to sea-air fluxes, Level 4 analyses adjusted the data to correspond to 20 cm depths that are comparable to the data obtained via drifting satellite-tracked instruments. The satellite radiances were harmonized between the sensors using several algorithms. For example, the effects of cloud and sea ice cover were addressed in constructing the sea surface temperatures.

Further, "optimal estimation" algorithms were employed for updating the signals from satellites [22] and utilized "reduced-state-space pseudo-maximum likelihood inverse" [19]. Note that 25,920,000 observations for 0.05 × 0.05-degree grids for sea surface temperatures were available for each of the 240 months during 2000–2019 [19]. The data were averaged for the 64,800 1 × 1-degree grids; averages were also created for the quarters for the statistical analyses. The data were checked for internal consistencies.

Next, radar altimetry data for sea ice concentrations, expressed as the percentages of the area of the grid covered by sea ice, were obtained via satellite signals for both hemispheres [18]. The "Level 3" monthly data were available for 648,000,000 0.01 × 0.01-degree grids and were averaged to produce the data for 64,800 1 × 1 degree grids that were merged with the data for sea surface temperatures. Note sea ice thicknesses data were available only for the Northern hemisphere; the remote sensing signals inferred the heights of ice above sea level (freeboard) and the snow depths were estimated based on signal delays [23,24]. The correlations between sea ice concentrations and thicknesses in the Northern hemisphere were high especially for greater levels of sea ice thickness. Moreover, in the ice-covered regions, sea surface temperatures were not interpolated as quadratic functions of sea ice thicknesses [33], affording the modelling of sea surface temperatures and sea ice concentrations interrelationships (Section 3).

Lastly, monthly data on the velocities of ocean surface currents were available for 0.33 × 0.33-degree grids from the ocean surface current analysis (OSCAR) [20]; the data were averaged for 1 × 1 degree grids and merged with the data for sea surface temperatures and sea ice concentrations. The near-surface zonal and meridional velocities were derived as nonlinear functions of sea surface heights, wind stress, sea surface displacement, depth, eddy viscosity, vertical sheer, and buoyancy force [32,34]. The absolute values of velocities over 3 m/s were dropped from the data set. Note that the buoyancy force was also a function of changes in weekly sea surface temperatures [35] that could in turn induce correlations between quarterly levels of sea surface temperatures and the error terms affecting empirical models for zonal and meridional velocities (Section 3). The eddy kinetic energy was computed for the quarters by summing the squared values of zonal and meridional velocities for the grids [30].

3. Modelling the Interrelationships between Sea Surface Temperatures, Sea Ice Concentrations and Ocean Surface Current Velocities

Longitudinal data are useful for modelling the dynamic interrelationships between climate indicators such as greenhouse gas emissions and concentrations, ambient temperatures, ocean acidification and deoxygenation, sea surface temperatures, sea ice concentrations and polar ice thickness, and ocean surface current velocities [7]. While in situ data are available for ocean acidification and deoxygenation from approximately 380,000 oceanographic stations [36], cryosphere measurements often need to rely on remote sensing signals. Moreover, nonlinear transformations are used for processing satellite signals, and it is sometimes necessary to incorporate the effects of the related variables. While Wiener [22] emphasized that groups of transformations applied to variables should be invariant with respect to shifts in time, this may not be feasible in nonlinear applications.

For example, partial differential equations for ocean dynamics are approximations for the complex and "chaotic" sea water movements [27,37]. If the data on "uncontaminated" variables are available, then it would be useful to test the validity of transformations using likelihood ratio or Wald [38] type statistics.

This paper develops empirical models for sea surface temperatures, sea ice concentrations, and ocean surface current velocities, tackling the interdependence between the variables and certain methodological aspects. First, dynamic models for sea surface temperatures containing past levels of the dependent variables were estimated using data for 1×1 degree grids in 20 quarters for the hemispheres. A complete set of time indicator variables for the years was included for taking into account differences in the time means. Moreover, for analyzing the effects of previous sea ice concentrations for current sea surface temperatures, static models without lagged dependent variables were estimated. This was partly because the estimation of dynamic models requires at least one time varying explanatory variable that is uncorrelated with the error terms (Section 3.2). Moreover, nonlinear transformations can affect dynamic properties of the variables and induce correlations between the explanatory variables and the errors affecting the models.

Second, static models were estimated for sea ice concentrations with sea surface temperatures included as an explanatory variable that could be correlated with the grid-specific random effects; dynamic aspects were captured by postulating unrestricted dispersion matrices for the errors affecting the static models. Third, the models for zonal and meridional velocities of ocean surface currents and eddy kinetic energy were estimated with sea surface temperatures included as an explanatory variable. Because the *changes* in weekly sea surface temperatures were utilized for constructing zonal and meridional ocean surface current velocities, errors affecting the models could be correlated with the quarterly levels of sea surface temperatures. Overall, for assessing the robustness of the empirical results, dynamic and static versions of the models were estimated for all the postulated relationships.

3.1. The Empirical Models

The model for the quarterly sea surface temperatures for the ith grid in time period t is given by:

$$\begin{aligned} \ln(\text{Sea surface temperatures})_{it} = {} & a_0 + a_1 \ln(\text{Latitude})_i + a_2 \ln(\text{Longitude})_i \\ & + a_3 (\text{Year } 2002)_t + a_4 (\text{Year } 2003)_t + a_5 (\text{Year } 2004)_t + a_6 (\text{Year } 2005)_t \\ & + a_7 (\text{Year } 2006)_t + a_8 (\text{Year } 2007)_t + a_9 (\text{Year } 2008)_t + a_{10} (\text{Year } 2009)_t \\ & + a_{11} (\text{Year } 2010)_t + a_{12} (\text{Year } 2011)_t + a_{13} (\text{Year } 2012)_t + a_{14} (\text{Year } 2013)_t \\ & + a_{15} (\text{Year } 2014)_t + a_{16} (\text{Year } 2015)_t + a_{17} (\text{Year } 2016)_t + a_{18} (\text{Year } 2017)_t \\ & + a_{19} (\text{Year } 2018)_t + a_{20} (\text{Year } 2019)_t + a_{21} \ln(\text{Sea surface temperatures})_{it-1} \\ & + u_{it} \ (i = 1,2, \ldots, N; t = 2, 3, \ldots, 20) \end{aligned} \quad (1)$$

Here, ln represents natural logarithms. Note that for using logarithmic transformations, sea surface temperatures can be expressed in Kelvin. Because the freezing point of sea water is -2 degrees centigrade, it was simpler to add two degrees to the temperatures in centigrade for circumventing the zero values. This transformation was also helpful for reducing heteroscedasticity in the data. The model in (1) was separately estimated for Northern and Southern hemispheres and the geodesic variables accounted for the regional characteristics. The dynamic model contained previous level of sea surface temperatures as an explanatory variable. In view of data availability for 20 quarters, at most, 18 time indicators for the years 2002–2019 were included in (1); the initial observations on sea surface temperatures were modeled using a "reduced form" that had its own constant term (see Equation (4) below).

The errors u_{it}'s affecting (2) can be decomposed in a simple random effects fashion as:

$$u_{i\,t} = \delta_i + v_{it} \ (i = 1,2, \ldots, N; t = 2,3, \ldots, T) \quad (2)$$

where δ_i were the grid-specific random effects that were assumed to be distributed with zero mean and constant variance, and v_{it} were distributed with zero mean and constant variance.

The static model for sea ice concentrations was similar to that in Equation (1) but with the previous level of sea ice concentrations excluded from the model. A set of 18 time indicator variables was included in this model though these variables are suppressed in Equation (3) for economizing on space:

$$\begin{gathered}\ln\,(\text{Sea ice concentrations})_{it} = b_0 + b_1 \ln\,(\text{Latitude})_i \\ + b_2 \ln\,(\text{Longitude})_i + \ldots + b_{21} \ln\,(\text{Sea surface temperatures})_{it} + u_{it} \\ (i = 1, 2, \ldots, N;\ t = 1, \ldots, 20)\end{gathered} \tag{3}$$

Note that the previous levels of sea surface temperatures were included in an alternative version of the model for sea ice concentrations for circumventing possible simultaneity problems. Additionally, the coefficients of the explanatory variables such as sea surface temperatures in (3) were the "elasticities" (percent change in the dependent variable resulting from one percent change in an explanatory variable). Lastly, the models for zonal and meridional velocities of ocean surface currents were similar to the model in Equation (3). In addition, models were estimated for the respective squares of the zonal and meridional velocities and for the sum of squared velocities, i.e., for eddy kinetic energy. Statistical criteria were employed for comparing the models for zonal and meridional velocities versus eddy kinetic energy (Section 7).

3.2. Statistical and Econometric Methods

The dynamic random effects models for sea surface temperatures were estimated by maximum likelihood methods, assuming that the number of grids (N) was large but number of time periods (T) was fixed [39]. The estimation techniques treated previous observations on dependent variables as "endogenous", i.e., correlated with the errors u_{it}. The errors affecting the models were assumed to be independent drawings from a multivariate normal distribution with a T × T symmetric positive definite dispersion matrix Ω.

For exposition purposes, dynamic models can be written in a simultaneous equations framework by defining a "reduced form" equation for initial observations and a "triangular" system of (T-1) "structural" equations for remaining time periods:

$$y_{i1} = \sum_{j=1}^{m} z_{ij}\zeta_j + \sum_{j=1}^{n}\sum_{k=1}^{T} \upsilon_{jk} X_{ijk} + u_{i1} \qquad (i = 1, \ldots N) \tag{4}$$

and

$$\underset{(T-1)\times T}{B}\ \underset{T\times N}{Y'} + \underset{(T-1)\times m}{C_1}\ \underset{m\times N}{Z'} + \underset{(T-1)\times nT}{C_2}\ \underset{nT\times N}{X'} = \underset{(T-1)\times N}{U'} \tag{5}$$

Here, Y, Z and X are, matrices containing, respectively, observations on the dependent, time invariant, and time varying explanatory variables; dimensions of the matrices are written below the respective symbols. B was a (T-1) × T lower triangular matrix of coefficients such that

$$B_{ii} = \alpha,\ B_{i,i+1} = -1,\ B_{ij} = 0\ \ otheriwse\ (i = 1, \ldots, T-1; j = 1, \ldots T) \tag{6}$$

where α was the coefficient of lagged dependent variable. The matrices C_1 and C_2 contained the coefficients of time invariant and time varying variables, respectively; the matrix U contained the error terms. The errors affecting the model in Equations (4) and (5) were assumed to be independent drawings from a multivariate normal distribution with a T × T symmetric positive definite dispersion matrix Ω. The "profile" or "concentrated" likelihood function for the model can be written as [39]:

$$\ln L^* = -0.5N \ln\det\,(W) + 0.5N \ln\det(B\ W\ B') - 0.5N \ln\det(\Omega_{22}) \tag{7}$$

where Ω_{22} was the (T−1) × (T−1) submatrix of Ω corresponding to Equation (5) and was a function of the unknown model parameters. W was a T × T matrix:

$$W = \left\{ (Y'Y) - Y'Z^* \left(Z^{*'} Z^* \right)^{-1} Z^{*'} Y \right\} / T \tag{8}$$

and Z^* was the matrix containing time invariant and time varying explanatory variables Z and X, respectively, i.e., Z^* = {Z: X}.

A numerical optimization routine (E04 JBF) [40] was used in a FORTRAN program for computing the parameters using the profile likelihood functions for the cases where the dispersion matrix Ω was unrestricted as in Equation (7), and where Ω corresponded to the random effects decomposition (2). The asymptotic standard errors of the parameters were computed by numerically approximating the second derivatives of the maximized log-likelihood functions.

Further, the static random effects models for sea ice concentrations and zonal and meridional velocities of ocean surface currents were estimated using efficient stepwise methods with the dispersion matrix Ω unrestricted [41]; see below). The estimation of dynamic models requires at least one time-varying variable in the model that was uncorrelated with the random effects which may be infeasible in some models due to the transformations used for processing the remote sensing signals. By contrast, static models can be estimated where all time varying explanatory variables might be correlated with the errors. The correlation pattern for dependence between an explanatory variable (x_2) and random effects (δ_i) was:

$$x_{2it} = \lambda \delta_i + x^*_{2it} \tag{9}$$

where x^*_{2it} was uncorrelated with δ_i, and λ was a scalar. This correlation pattern has the advantage that the deviations of x_{2it} from the time mean:

$$x^+_{2it} = x_{2it} - \overline{x}_{2i} \;\; (t = 2, \ldots, T;\; i = 1, \ldots, N) \tag{10}$$

$$\overline{x}_{2i} = \sum_{t=1}^{T} x_{2it} / T \;\; (i = 1, \ldots, N) \tag{11}$$

can be used as (T−1) "instrumental" variables for facilitating identification and the estimation of the parameters. Chi-squared tests were applied for the exogeneity hypothesis for certain explanatory variables by testing if the correlations between the errors (u_{it}) and the time means were zero. For example, with 20 quarterly observations on sea surface temperatures in Equation (3), the test statistic was distributed under the null hypothesis as a Chi-squared variable with 20 degrees of freedom.

Lastly, the assumption of normality of errors was not critical for "quasi" maximum likelihood estimates of the dynamic models computed under multivariate normality assumption. The estimated model parameters are consistent and asymptotically normally distributed provided that (4 + ε)th order moments (ε > 0) of the actual distribution function of errors exist [42–44]. Note that the normality assumptions were not necessary for static models because the criterion function minimized was the trace of a matrix:

$$\text{tr}\, \{\Omega^{-1}\, (A\, R\, A')\} \tag{12}$$

where the matrix A contained the coefficients in Equation (5) and R was a T × T matrix containing the second moments of the "predicted" parts of the variables in (5) using instrumental variables. Lastly, while one could estimate models with 'fixed effects' using data for large number of grids for a few time periods, the increase in the number of dummy variables with sample size leads to the problem of 'incidental parameters' [45].

4. Results

Descriptive Statistics and t-Tests for Sea Surface Temperatures, Sea Ice Concentrationses and Ocean Surface Current Velocities

Table 1 reports the quarterly sample means and standard deviations of the sea surface temperatures, sea ice concentrations, and zonal and meridional velocities of ocean surface currents for 1 × 1 degree grids for the subset of years 2000, 2003, 2006, 2009, 2012, 2015, 2017, and 2019 using the available data for the Northern hemisphere. The corresponding results for the Southern hemisphere are in Table 2. Significant changes in the variables between 2000 and 2019 from the applications of paired *t*-test statistics are marked in Tables 1 and 2. First, in Table 1, the sample means of sea surface temperatures showed upward trends in all quarters. Moreover, Figure 1 displays the changes in sea surface temperatures and sea ice concentrations between 2000 and 2019 for the four quarters in the Northern and Southern hemispheres that were all statistically significant. The increases in sea surface temperatures for the quarters were quite gradual and were greater in the Northern hemisphere. By contrast, there were greater fluctuations in the changes in sea ice concentrations across the quarters and the concentrations were reduced between 2000 and 2019 in both hemispheres.

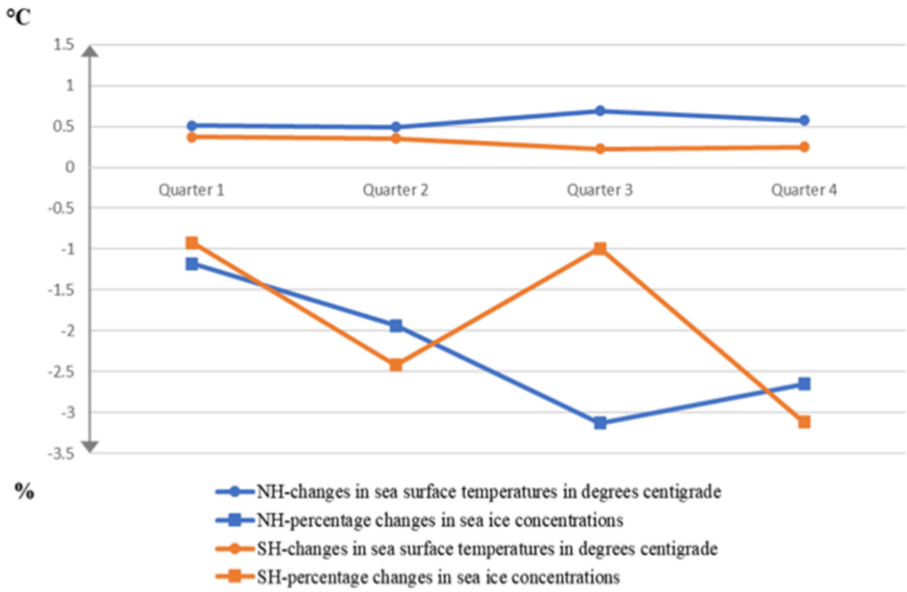

Figure 1. Changes in sea surface temperatures and sea ice concentrations between 2000 and 2019 in the four quarters in the Northern and Southern hemispheres using data for 1×1 degree grids.

Second, the zonal and meridional velocities of ocean surface currents did not exhibit clear trends during the sample period. The changes between 2000 and 2019 were negative and significant for zonal velocities in second and fourth quarters, whereas the changes were positive and significant for meridional velocities in second, third and fourth quarters. Note that for the year 2000, the data were utilized for 13,734, 10,281, 12,398 and 12,407 grids, respectively, for the sea surface temperatures, sea ice concentrations, and zonal and meridional velocities.

Table 1. Sample means and standard deviations of quarterly sea surface temperatures, sea ice concentrations, and zonal and meridional ocean current velocities for 1 × 1 degree grids in the Northern hemisphere during 2000–2019 [1,2].

Year:	2000		2003		2006		2009		2012		2015		2017		2019	
Variables:	**Mean**	**SD**	**Mean**	**SD**	**Mean**	**SD**	**Mean**	**SD**	**Mean**	**SD**	**Mean**	**SD**	**Mean**	**SD**	**Mean**	**SD**
Quarter 1:																
Sea surface temp, °C	16.79	10.36	12.63	12.16	12.65	12.04	12.59	12.03	12.61	12.03	12.77	12.12	12.81	12.18	12.86 +	12.18
Sea ice concens., %	44.47	47.14	44.73	46.93	43.26	47.03	44.40	47.36	43.31	47.05	44.04	47.74	42.04	46.36	43.29 +	47.25
Zonal velocity, m/s	−0.021	0.130	−0.032	0.145	−0.029	0.137	−0.028	0.130	−0.019	0.122	−0.014	0.145	−0.024	0.135	−0.020	0.135
Meridional veloc., m/s	0.014	0.088	0.014	0.090	0.016	0.086	0.016	0.085	0.016	0.087	0.015	0.085	0.016	0.083	0.013	0.085
Quarter 2:																
Sea surface temp, °C	16.34	11.33	13.19	12.48	13.18	12.41	13.18	12.42	13.21	12.39	13.40	12.55	13.38	12.56	13.47 +	12.57
Sea ice concens., %	43.41	46.66	43.68	46.51	41.61	46.09	43.27	46.56	43.30	46.03	42.12	46.45	42.14	46.29	41.48 +	45.98
Zonal velocity, m/s	0.001	0.148	−0.005	0.133	0.005	0.134	0.009	0.132	0.009	0.130	0.012	0.145	−0.005	0.122	−0.005 +	0.126
Meridional veloc., m/s	0.014	0.086	0.014	0.089	0.014	0.086	0.012	0.086	0.011	0.083	0.012	0.083	0.012	0.083	0.009 +	0.083
Quarter 3:																
Sea surface temp, °C	18.37	11.04	15.75	12.45	15.72	12.37	15.76	12.45	15.80	12.23	16.03	12.50	15.93	12.47	16.21 +	12.45
Sea ice concens., %	29.27	37.69	30.03	39.17	29.83	40.46	29.01	39.45	24.98	36.17	27.78	38.67	26.95	37.39	26.15 +	37.30
Zonal velocity, m/s	0.005	0.139	0.015	0.147	0.019	0.153	0.015	0.146	0.010	0.146	0.019	0.173	−0.001	0.145	0.003	0.157
Meridional veloc., m/s	0.011	0.092	0.011	0.094	0.011	0.091	0.011	0.089	0.010	0.091	0.006	0.089	0.009	0.092	0.007 +	0.089
Quarter 4:																
Sea surface temp, °C	17.53	11.30	14.81	12.55	14.89	12.49	14.76	12.59	14.85	12.43	15.12	12.69	14.97	12.56	15.13 +	12.62
Sea ice concens., %	34.65	43.98	35.98	43.55	35.03	43.52	33.16	41.62	31.30	40.51	33.01	41.60	32.71	41.77	32.00 +	41.04
Zonal velocity, m/s	−0.012	0.150	0.001	0.150	0.004	0.144	0.010	0.140	−0.005	0.143	0.007	0.153	−0.014	0.156	−0.004 +	0.128
Meridional veloc., m/s	0.015	0.089	0.014	0.091	0.016	0.086	0.012	0.087	0.014	0.088	0.013	0.083	0.014	0.085	0.009 +	0.080

[1] Quarterly data for 20 years were used for up to 32,400 1 × 1 degree grids in the Northern hemisphere for computing sample means and standard deviations; results are reported for selected years for economizing on space. [2] Quarterly data were available in year 2000 for sea surface temperatures, sea ice concentrations, and zonal and meridional velocities for, respectively, 13,734, 10,281, 12,398, and 12,407 grids. + Paired *t*-tests were significant ($p < 0.05$) for changes in the variables between 2000 and 2019.

Table 2. Sample means and standard deviations of quarterly sea surface temperatures, sea ice concentrations, and zonal and meridional ocean current velocities for 1 × 1 degree grids in the Southern hemisphere during 2000–2019 [1,2].

Year:	2000		2003		2006		2009		2012		2015		2017		2019	
Variables:	**Mean**	**SD**	**Mean**	**SD**	**Mean**	**SD**	**Mean**	**SD**	**Mean**	**SD**	**Mean**	**SD**	**Mean**	**SD**	**Mean**	**SD**
Quarter 1:																
Sea surface temp, °C	15.04	10.85	15.16	10.81	15.20	10.74	15.11	10.90	15.01	10.78	15.19	10.96	15.46	10.78	15.37 +	10.93
Sea ice concens., %	5.13	16.81	6.61	20.28	4.37	15.93	5.70	17.83	5.91	18.44	6.61	19.12	3.78	14.92	4.20 +	16.04
Zonal velocity, m/s	0.015	0.109	0.008	0.120	0.009	0.118	0.012	0.110	0.015	0.104	0.016	0.112	0.012	0.116	0.0150	0.108
Meridional veloc., m/s	0.001	0.075	0.002	0.072	0.001	0.073	0.001	0.075	0.001	0.074	0.003	0.073	0.001	0.071	0.003	0.070
Quarter 2:																
Sea surface temp, °C	14.44	10.99	14.46	11.01	14.43	11.02	14.46	11.11	14.42	11.01	14.52	11.15	14.70	11.07	14.68 +	11.15
Sea ice concens., %	12.60	27.86	12.93	28.87	11.19	25.85	13.19	28.92	12.38	27.97	13.79	29.59	9.75	23.69	10.18 +	24.96
Zonal velocity, m/s	0.012	0.113	0.006	0.116	0.012	0.112	0.015	0.109	0.016	0.110	0.015	0.115	0.010	0.114	0.010 +	0.115
Meridional veloc., m/s	−0.001	0.076	0.002	0.074	0.002	0.074	0.0001	0.075	−0.001	0.071	0.001	0.074	−0.001	0.073	0.002 +	0.072
Quarter 3:																
Sea surface temp, °C	13.36	10.14	12.49	10.55	12.43	10.51	12.53	10.58	12.57	10.55	12.57	10.63	12.63	10.58	12.64 +	10.59
Sea ice concens., %	23.14	38.73	22.63	38.21	22.90	38.56	22.91	38.20	23.12	38.43	23.28	38.80	21.26	37.02	22.15 +	37.88
Zonal velocity, m/s	0.002	0.113	0.003	0.116	0.005	0.121	0.001	0.122	0.005	0.118	0.006	0.115	−0.001	0.126	0.004	0.119
Meridional veloc., m/s	−0.002	0.078	0.002	0.078	0.001	0.075	−0.001	0.076	−0.002	0.077	0.0001	0.076	−0.002	0.079	0.001 +	0.074
Quarter 4:																
Sea surface temp, °C	13.00	10.59	12.86	10.70	12.78	10.70	12.89	10.73	12.92	10.72	13.00	10.85	12.91	10.67	12.99 +	10.75
Sea ice concens., %	23.65	39.08	20.86	35.35	21.24	35.64	21.10	35.57	21.57	36.02	21.34	36.13	20.09	34.73	20.54 +	35.41
Zonal velocity, m/s	0.009	0.114	0.014	0.117	0.010	0.114	0.019	0.111	0.013	0.114	0.017	0.106	0.011	0.126	0.013 +	0.106
Meridional veloc., m/s	−0.001	0.076	−0.001	0.078	−0.001	0.077	−0.001	0.076	−0.001	0.077	0.001	0.076	−0.001	0.075	0.001 +	0.070

[1] Quarterly data for 20 years were used for up to 32,400 1 × 1 degree grids in the Southern hemisphere for computing sample means and standard deviations. [2] Quarterly data were available in year 2000 for sea surface temperatures, sea ice concentrations, and zonal and meridional velocities for, respectively, 21,760, 12,931, 21,032, and 21,034 grids. + Paired *t*-tests were significant ($p < 0.05$) for changes in the variables between 2000 and 2019.

The sample means and standard deviations of sea surface temperatures, sea ice concentrations and zonal and meridional velocities of ocean surface currents for the Southern hemisphere in Table 2 were similar to those for the Northern hemisphere. The data were available for greater numbers of grids in the Southern hemisphere and there were significant increases in sea surface temperatures between 2000 and 2019 for all quarters and significant declines in sea ice concentrations. The changes between 2000 and 2019 in the zonal velocities were positive and significant in second and fourth quarters, whereas they were positive and significant for meridional velocities in second, third, and fourth quarters. Overall, the zonal and meridional velocities in the hemispheres were small in magnitudes and there were zero values recorded for one of the two velocities for many grids. By contrast, sample means of eddy kinetic energy for the quarters in the hemispheres were larger and showed significant increase between 2000 and 2019 in the Northern hemisphere; changes in the Southern hemisphere were not statistically significant. These results are not reported in Tables 1 and 2 for economizing on space but are discussed in Section 7 when interpreting the findings from the models for zonal and meridional velocities and eddy kinetic energy.

5. Empirical Results from the Models for Quarterly Sea Surface Temperatures in the Hemispheres

Table 3 presents the maximum likelihood estimates of model for the sea surface temperatures using data on over 14,500 1 × 1 degree grids for 40 quarters in 2000–2019 in the Northern hemisphere. The sea surface temperatures in centigrade were transformed into natural logarithms after adding two degrees for circumventing zero values. First, the coefficients of the indicator variables for years were invariably positive and significant ($p < 0.05$) in all models for the quarters; the only exceptions were in 2002 for the first and fourth quarters. These results support the findings from the sample means in Table 1 and Figure 1 showing significant increases in sea surface temperatures during the sample period. Second, the estimated coefficients of the latitude variables were negative and significant in all models indicating declines in temperatures at higher latitudes. The estimated coefficients of longitudes were positive for first three quarters but the coefficient was negative in the fourth quarter; these coefficients depend on several factors and may not afford simple comparisons.

Third, the coefficients of the lagged dependent variables in the four models were between 0.16 for the third quarter to 0.38 for the first quarter and were all statistically significant. The magnitudes of the coefficients imply that the long run elasticities of sea surface temperatures with respect to (say) latitudes of the grids were approximately 1.33 times greater than the corresponding short run elasticities reported in Table 3. The between-to-within grid variance ratios were large and were in the interval (32.38, 65.34) indicating the importance of location for the sea surface temperatures. The within-grid variances were similar in the four quarters though the variance was higher in third quarter corresponding to summer in the Northern hemisphere. Note that while the likelihood ratio statistics generally favored models with an unrestricted dispersion matrix Ω over the simple random effects decomposition in (2), the empirical results were similar and the between and within grid variances in Tables 3 and 4 provide useful insights.

Lastly, sea ice concentrations in the previous quarters were included in static versions of the models for sea surface temperatures, allowing for possible correlations between the previous sea ice concentrations and the random effects (δ_i). In all models, the estimated coefficients of previous sea ice concentrations were negative and statistically significant. The estimated elasticities of the sea surface temperatures with respect to previous sea ice concentrations for the quarters were −0.075, −0.075, −0.046, and −0.049, respectively. The Chi-squared statistics often rejected the null hypotheses of zero correlations between the random effects and sea ice concentrations in the previous quarter. These results indicate the presence of feedback effects, i.e., reductions in the levels of sea ice concentrations imply higher sea surface temperatures in subsequent quarters (Section 8).

Table 3. Maximum likelihood estimates of dynamic random effects models using quarterly data for 2000–2019 for 1 × 1 degree grids on sea surface temperatures in the Northern hemisphere explained by geodesic variables and time indicators for the years [1].

Dependent Variable:	**ln (Sea Surface Temperatures +2), °C**							
	Quarter 1		**Quarter 2**		**Quarter 3**		**Quarter 4**	
Explanatory variables:	Coefficient	SE	Coefficient	SE	Coefficient	SE	Coefficient	SE
Constant	15.311	0.075	15.359	0.059	2.461	0.009	4.138	0.012
ln (Latitude), 0–180	−3.020 *	0.013	−3.059 *	0.008	−0.145 *	0.002	−0.466 *	0.001
ln (Longitude), 0–360	0.119 *	0.002	0.207 *	0.005	0.071 *	0.001	−0.028 *	0.002
Year 2002, 0–1	−0.001	0.001	0.021 *	0.001	0.005 *	0.002	−0.005 *	0.002
Year 2003, 0–1	0.006 *	0.001	0.008 *	0.001	0.001	0.003	0.006 *	0.002
Year 2004, 0–1	0.012 *	0.001	0.031 *	0.001	0.020 *	0.003	0.012 *	0.002
Year 2005, 0–1	0.027 *	0.001	0.031 *	0.001	0.034 *	0.003	0.027 *	0.002
Year 2006, 0–1	0.024 *	0.001	0.030 *	0.001	0.017 *	0.003	0.017 *	0.002
Year 2007, 0–1	0.014 *	0.001	0.020 *	0.001	0.090 *	0.002	0.070 *	0.002
Year 2008, 0–1	0.007 *	0.001	0.018 *	0.001	0.021 *	0.003	0.012 *	0.002
Year 2009, 0–1	0.008 *	0.001	0.021 *	0.001	0.033 *	0.003	0.015 *	0.002
Year 2010, 0–1	0.026 *	0.001	0.028 *	0.001	0.050 *	0.003	0.030 *	0.002
Year 2011, 0–1	0.021 *	0.001	0.029 *	0.001	0.062 *	0.003	0.053 *	0.002
Year 2012, 0–1	0.013 *	0.001	0.028 *	0.001	0.085 *	0.003	0.075 *	0.002
Year 2013, 0–1	0.022 *	0.001	0.025 *	0.001	0.046 *	0.003	0.018 *	0.002
Year 2014, 0–1	0.030 *	0.001	0.036 *	0.001	0.069 *	0.003	0.041 *	0.002
Year 2015, 0–1	0.023 *	0.001	0.047 *	0.001	0.077 *	0.003	0.056 *	0.002
Year 2016, 0–1	0.041 *	0.001	0.064 *	0.001	0.087 *	0.003	0.071 *	0.002
Year 2017, 0–1	0.036 *	0.001	0.033 *	0.001	0.050 *	0.002	0.042 *	0.002
Year 2018, 0–1	0.042 *	0.001	0.048 *	0.001	0.055 *	0.002	0.073 *	0.002
Year 2019, 0–1	0.034 *	0.001	0.082 *	0.001	0.161 *	0.002	0.083 *	0.002
Lagged dependent variable	0.380 *	0.001	0.259 *	0.001	0.163 *	0.001	0.235 *	0.001
Between/within variance, n	39.387 *	0.290	65.343 *	0.300	32.380 *	0.278	47.867 *	0.221
Within variance, n	0.0120		0.0142		0.0431		0.0262	
2 × Max. log-likelihood fn.	1,178,232.34		114,032.40		855,311.33		1,003,383.16	
Number of grids	14,457		14,661		15,180		15,225	
ln(Lagged sea ice concens.),% [2]	−0.075 *	0.001	−0.075 *	0.001	−0.046 *	0.001	−0.049 *	0.001

[1] Slope coefficients and standard errors are reported using 20 quarterly observations on 1 × 1 degree grids for sea surface temperatures in the Northern hemisphere. [2] Static random effects models that included previous sea ice concentrations as an explanatory variable were estimated using 19 quarterly observations for investigating the feedback effects. * $p < 0.05$.

Table 4. Maximum likelihood estimates of dynamic random effects models using quarterly data for 2000–2019 for 1 × 1 degree grids on sea surface temperatures in the Southern hemisphere explained by geodesic variables and time indicators for the years [1].

Dependent Variable:	**ln (Sea Surface Temperatures +2), °C**							
	Quarter 1		**Quarter 2**		**Quarter 3**		**Quarter 4**	
Explanatory variables:	Coefficient	SE	Coefficient	SE	Coefficient	SE	Coefficient	SE
Constant	−1.309	0.014	−7.471	0.020	−10.473	0.035	−114.335	0.024
ln (Latitude), 0–180	1.107 *	0.004	2.473 *	0.006	3.071 *	0.009	3.261 *	0.006
ln (Longitude), 0–360	−0.156 *	0.001	−0.005 *	0.001	0.064 *	0.001	0.116 *	0.001
Year 2002, 0–1	−0.007 *	0.001	−0.004 *	0.001	0.007 *	0.002	0.013 *	0.001
Year 2003, 0–1	−0.001	0.001	0.003 *	0.001	−0.001	0.001	0.005 *	0.001
Year 2004, 0–1	−0.008 *	0.001	−0.015 *	0.001	−0.008 *	0.001	0.002 *	0.001
Year 2005, 0–1	0.014 *	0.001	−0.008 *	0.001	−0.007 *	0.001	−0.001	0.001
Year 2006, 0–1	0.029 *	0.001	0.009 *	0.001	−0.007 *	0.003	−0.002 *	0.001
Year 2007, 0–1	−0.006 *	0.001	−0.001	0.001	−0.005 *	0.001	−0.009 *	0.001
Year 2008, 0–1	−0.039 *	0.001	−0.036 *	0.001	−0.006 *	0.001	−0.004 *	0.001
Year 2009, 0–1	−0.012 *	0.002	−0.013 *	0.001	0.0004	0.001	0.011 *	0.001
Year 2010, 0–1	0.018 *	0.001	0.010 *	0.001	−0.007 *	0.001	−0.006 *	0.001
Year 2011, 0–1	−0.0001	0.002	−0.005 *	0.001	0.0002	0.001	0.005 *	0.001
Year 2012, 0–1	−0.024 *	0.002	−0.008 *	0.001	0.008 *	0.001	0.009 *	0.001
Year 2013, 0–1	0.014 *	0.001	−0.006 *	0.001	−0.004 *	0.001	−0.007 *	0.001
Year 2014, 0–1	−0.010 *	0.001	−0.020 *	0.001	−0.007 *	0.001	−0.001	0.001
Year 2015, 0–1	−0.027 *	0.001	−0.019 *	0.001	−0.002 *	0.001	0.004 *	0.001
Year 2016, 0–1	−0.001	0.001	−0.003 *	0.001	0.010 *	0.001	0.033 *	0.001
Year 2017, 0–1	0.061 *	0.002	0.048 *	0.001	0.020 *	0.001	0.010 *	0.001
Year 2018, 0–1	0.014 *	0.001	0.013 *	0.001	0.010 *	0.001	0.013 *	0.001
Year 2019, 0–1	0.032 *	0.001	0.028 *	0.001	0.119 *	0.001	0.035 *	0.001
Lagged dependent variable	0.126 *	0.001	0.111 *	0.001	0.139 *	0.001	0.083 *	0.001
Between/within variance, n	27.598 *	0.134	25.566 *	0.077	51.352 *	0.100	37.077 *	0.105
Within variance, n	0.0192		0.0088		0.0068		0.0093	
2 × Max. log-likelihood fn.	1,595,576.69		1,935,711.25		2,037,505.15		1,907,332.67	
Number of grids	21,929		21,892		21,939		21,921	
ln(Lagged sea ice concens.),% [2]	−0.026 *	0.001	−0.019 *	0.001	−0.048 *	0.001	−0.058 *	0.001

[1] Slope coefficients and standard errors are reported using 20 quarterly observations on 1 × 1 degree grids for sea surface temperatures in the Southern hemisphere. [2] Static random effects models that included previous sea ice concentrations as an explanatory variable were estimated using 19 quarterly observations for investigating the feedback effects. * $p < 0.05$.

The empirical results for the Southern hemisphere in Table 4 using the data on over 21,892 grids were similar in many respects to the results for the Northern hemisphere. However, there were certain differences as well. For example, coefficients of the latitude variables were positive and significant for all quarters, as would be expected. More importantly, coefficients of the indicator variables for the years were often estimated with negative signs that were statistically significant indicating greater cyclical patterns in the sea surface temperatures. Such patterns would be obscured in models pooling the data for the hemispheres. Note, however, that for more recent years 2017–2019, the estimated coefficients were positive and significant indicating higher sea surface temperatures. This may also be due to a tendency for equalization of sea surface temperatures in the hemispheres via ocean currents (Sections 7 and 8).

6. Empirical Results from the Models for Sea Ice Concentrations in the Hemispheres

Table 5 reports the results from estimating static models for sea ice concentrations using the data for a subset of 2761 grids with non-zero values in at least one of the 40 quarters in the Northern hemisphere; the zero values for some of the quarters were set to 0.01 prior to the logarithmic transformations. First, the coefficients of the latitude variable were estimated with negative signs in the first quarter, whereas these coefficients were positive in the third and fourth quarters. The models indicated certain nonlinearities with respect to the latitudes of the grids. In contrast, the coefficients of the longitudes of the grids were small and statistically significant for the third and fourth quarters. Second, the estimated coefficients of time indicators for the years were negative and statistically significant for most quarters indicating significant declines in sea ice concentrations. While some of the coefficients of the time indicator variables were positive, they were generally small in magnitudes.

Third, estimated elasticities of sea ice concentrations with respect to sea surface temperatures in the four quarters were −2.23, −1.83, −1.22, and −0.859, respectively. All these coefficients were statistically significant and implied proportionately greater declines in sea ice concentrations with increases in sea surface temperatures [46]. The estimated elasticities were reduced by approximately 33 percent when alternative versions of the models replaced the current sea surface temperatures with the temperatures in the previous quarter. This may have been partly due to the cyclical patterns in sea surface temperatures. The Chi-squared tests rejected the null hypotheses that the random effects affecting the model for sea ice concentrations were uncorrelated with the sea surface temperatures, and the estimation methods took into account the underlying correlations.

Lastly, the results in Table 6 for the Southern hemisphere were similar to those for the Northern hemisphere. However, coefficients of the indicator variables for the years were often positive especially for the first quarter. In general, some of these coefficients were positive while others were negative indicating greater cyclical patterns in the Southern hemisphere. The elasticities of sea ice concentrations with respect to sea surface temperatures for the quarters were −3.24, −2.66, −2.94, and −3.00, respectively. These were somewhat larger than the corresponding estimates for the Northern hemisphere indicating that the increases in the sea surface temperatures were likely to reduce sea ice concentrations (Section 8).

Table 5. Efficient estimates of static random effects models using quarterly data for 2000–2019 for 1 × 1 degree grids on sea ice concentrations in the Northern hemisphere explained by geodesic variables, time indicators for the years, and sea surface temperatures [1,2].

Dependent Variable:	**ln (Sea Ice Concentrations), %**							
	Quarter 1		**Quarter 2**		**Quarter 3**		**Quarter 4**	
Explanatory variables:	Coefficient	SE	Coefficient	SE	Coefficient	SE	Coefficient	SE
Constant	6.432	2.588	1.125	2.679	−23.592	4.663	−159.172	4.374
ln (Latitude), 0–180	−3.072 *	0.513	0.108	0.531	5.186 *	0.916	31.723 *	0.861
ln (Longitude), 0–360	0.013	0.020	−0.021	0.019	−0.071 *	0.023	−0.198 *	0.024
Year 2002, 0–1	−0.031	0.031	−0.037	0.028	0.092 *	0.035	0.145 *	0.033
Year 2003, 0–1	0.052	0.037	0.066 *	0.031	0.167	0.039	0.044	0.027
Year 2004, 0–1	−0.118 *	0.038	−0.093 *	0.030	0.122 *	0.034	0.174 *	0.030
Year 2005, 0–1	−0.299 *	0.036	−0.181 *	0.028	0.067 *	0.033	0.053	0.030
Year 2006, 0–1	−0.194 *	0.037	−0.215 *	0.030	−0.323 *	0.034	−0.320 *	0.034
Year 2007, 0–1	−0.268 *	0.033	−0.227 *	0.029	0.114 *	0.040	−0.110 *	0.037
Year 2008, 0–1	−0.101 *	0.040	−0.027	0.033	0.038 *	0.033	0.156 *	0.028
Year 2009, 0–1	−0.101 *	0.034	0.034	0.032	−0.011	0.049	−0.190 *	0.032
Year 2010, 0–1	−0.197 *	0.037	0.144 *	0.026	−0.271 *	0.037	−0.124 *	0.037
Year 2011, 0–1	−0.226 *	0.039	−0.039	0.030	−0.020	0.042	−0.121 *	0.033
Year 2012, 0–1	−0.201 *	0.040	0.078 *	0.032	−0.367 *	0.047	−0.198 *	0.035
Year 2013, 0–1	−0.155 *	0.037	−0.075 *	0.026	−0.126 *	0.037	0.018	0.027
Year 2014, 0–1	−0.197 *	0.036	−0.116 *	0.032	−0.166 *	0.042	0.067	0.037
Year 2015, 0–1	−0.309 *	0.038	−0.195 *	0.036	0.040	0.039	−0.212 *	0.034
Year 2016, 0–1	−0.435 *	0.037	−0.183 *	0.033	−0.393 *	0.045	−0.669 *	0.040
Year 2017, 0–1	−0.249 *	0.040	−0.189 *	0.034	−0.171 *	0.037	−0.267 *	0.035
Year 2018, 0–1	−0.300 *	0.039	−0.175 *	0.032	−0.322 *	0.043	−0.220 *	0.037
Year 2019, 0–1	−0.086 *	0.033	0.090 *	0.035	0.238 *	0.046	−0.146 *	0.041
ln(Sea surface temperature+2),°C	−2.231 *	0.022	−1.834 *	0.019	−1.218 *	0.014	−0.859 *	0.015
Number of grids	2761		2919		2831		2858	

[1] Slope coefficients and standard errors are reported using 20 quarterly observations on 1 × 1 degree grids for sea ice concentrations in the Northern hemisphere. [2] Sea Surface temperatures were assumed to be correlated with grid-specific random effects. * $p < 0.05$.

Table 6. Efficient estimates of static random effects models using quarterly data for 2000–2019 for 1 × 1 degree grids on sea ice concentrations in the Southern hemisphere explained by geodesic variables, time indicators for the years, and sea surface temperatures [1,2].

Dependent Variable:	**ln (Sea Ice Concentrations), %**							
	Quarter 1		**Quarter 2**		**Quarter 3**		**Quarter 4**	
Explanatory variables:	Coefficient	SE	Coefficient	SE	Coefficient	SE	Coefficient	SE
Constant	3.016	0.503	3.825	0.608	1.099	0.337	1.105	0.239
ln (Latitude), 0–180	−1.139 *	0.172	−1.204 *	0.203	−0.444 *	0.108	−0.524 *	0.075
ln (Longitude), 0–360	0.166 *	0.026	0.137 *	0.027	0.038 *	0.017	0.052 *	0.011
Year 2002, 0–1	0.224 *	0.046	−0.386 *	0.041	−0.117 *	0.025	0.003	0.023
Year 2003, 0–1	0.354 *	0.047	0.372 *	0.036	0.062 *	0.027	0.130 *	0.027
Year 2004, 0–1	0.274 *	0.043	0.060 *	0.031	−0.069 *	0.028	0.024	0.024
Year 2005, 0–1	0.368 *	0.043	0.032	0.034	−0.113 *	0.027	0.101 *	0.023
Year 2006, 0–1	0.185 *	0.048	0.147 *	0.040	−0.041	0.025	0.142 *	0.022
Year 2007, 0–1	0.079	0.043	0.070 *	0.034	−0.012	0.026	0.115 *	0.025
Year 2008, 0–1	0.864 *	0.047	0.0013	0.032	−0.107 *	0.022	−0.056 *	0.023
Year 2009, 0–1	0.452 *	0.048	0.194 *	0.041	0.087 *	0.026	0.114 *	0.021
Year 2010, 0–1	0.540 *	0.047	0.497 *	0.034	0.013	0.027	0.042 *	0.024
Year 2011, 0–1	0.346 *	0.051	0.219 *	0.039	0.043	0.025	0.115 *	0.023
Year 2012, 0–1	0.201 *	0.052	−0.075 *	0.036	0.155 *	0.027	0.287 *	0.021
Year 2013, 0–1	0.266 *	0.045	0.229 *	0.041	0.137 *	0.026	0.228 *	0.022
Year 2014, 0–1	0.628 *	0.048	0.347 *	0.037	0.247 *	0.023	0.200 *	0.023
Year 2015, 0–1	0.789 *	0.045	0.292 *	0.039	−0.048 *	0.025	−0.037	0.023
Year 2016, 0–1	0.086 *	0.045	−0.177 *	0.040	−0.123 *	0.025	−0.026	0.023
Year 2017, 0–1	0.038	0.045	−0.028	0.038	−0.197 *	0.030	−0.147 *	0.027
Year 2018, 0–1	0.146 *	0.045	−0.190 *	0.038	−0.041	0.025	−0.020 *	0.022
Year 2019, 0–1	−0.217 *	0.048	0.350 *	0.042	0.014	0.029	0.265 *	0.022
ln(Sea surface temperature+2), °C	−3.236 *	0.022	−2.659 *	0.031	−2.935 *	0.025	−3.004 *	0.020
Number of grids	2882		3225		4361		4456	

[1] Slope coefficients and standard errors are reported using 20 quarterly observations on 1 × 1 degree grids for sea ice concentrations in the Southern hemisphere. [2] Sea Surface temperatures were assumed to be correlated with grid-specific random effects. * $p < 0.05$.

7. Empirical Results from the Models for Zonal and Meridional Velocities and Eddy Kinetic Energy of Ocean Surface Currents

Table 7 presents the results from estimating static models for the zonal and meridional velocities of ocean surface currents and for the eddy kinetic energy in the Northern hemisphere. The time indicator variables for the years were included in all models, though their coefficients were often statistically insignificant and are not reported. The corresponding results for the Southern hemisphere are in Table 8. First, the coefficients of the latitude variable for zonal velocities were positive and significant in the first and second quarters, while they were not statistically different from zero in the third and fourth quarters. By contrast, coefficients of latitudes were negative and significant in the models for meridional velocities in first, second, and fourth quarters. Moreover, coefficients of latitudes were negative in the first, second, and third quarters in the models for eddy kinetic energy. Second, the coefficients of the sea surface temperatures were positive and significant in the first and second quarters for zonal velocities. For the meridional velocities, this coefficient was negative and significant only in the first quarter. By contrast, coefficients of the sea surface temperatures were positive and significant in first, second, and fourth quarters in the models for eddy kinetic energy. As noted in Section 4, there were significant increases in the mean eddy kinetic energy between 2000 and 2019 in the Northern hemisphere.

Third, while likelihood ratio statistics cannot be easily applied for comparing the models for zonal and meridional velocities versus eddy kinetic energy, using the estimated within-grid variances as the decision criterion, the models for eddy kinetic energy generally had better fits. For example, in dynamic models for the zonal and meridional velocities and eddy kinetic energy, within-grid variances for these three climate indicators in the four quarters were {0.0067, 0.0036, 0.0013}, {0.0082, 0.0041, 0.0016}, {0.0090, 0.0044, 0.0028}, and {0.0084, 0.0041, 0.0019}, respectively. Thus, within-grid variances for eddy kinetic energy were at least 33 percent lower than those for the zonal and meridional velocities. This was perhaps not surprising because the correlations between zonal and meridional velocities were approximately 0.031, and the eddy kinetic energy was the complex conjugate (or squared modulus) of the velocities. Fourth, the fourth order moments of fitted residuals in the models for eddy kinetic energy in the first quarter were in the interval (33.53, 197.99) exceeding the values 3 for the normal distribution. However, the corresponding fourth order moments for logarithms of eddy kinetic energy were in the interval (5.21, 22.48). Because the estimated coefficients of sea surface temperatures were similar in these models, modelling the eddy kinetic energy seemed preferable to the zonal and meridional velocities.

Lastly, the results for zonal and meridional velocities and eddy kinetic energy for the Southern hemisphere are reported in Table 8. The coefficients of the latitude variable were negative and were statistically significant in the models for zonal velocity in all quarters; these coefficients were significant for the meridional velocities in the second and fourth quarters. By contrast, coefficients of the latitudes were positive and significant in all the models for eddy kinetic energy. Moreover, the coefficients of sea surface temperatures were generally negative in the models, especially for eddy kinetic energy. The latter was in contrast with the results for Northern hemisphere where sea surface temperatures were positively associated with the eddy kinetic energy. Such issues are revisited in Section 8.

Table 7. Efficient estimates of static random effects models using quarterly data for 2000–2019 for 1 × 1 degree grids on zonal and meridional ocean surface current velocities and eddy kinetic energy in the Northern hemisphere explained by geodesic variables, time indicators for the years, and sea surface temperatures [1,2,3].

Dependent Variable:	**Zonal Velocities, m/s**							
	Quarter 1		**Quarter 2**		**Quarter 3**		**Quarter 4**	
Explanatory variables:	Coefficient	SE	Coefficient	SE	Coefficient	SE	Coefficient	SE
Constant	−1.769	0.114	−0.397	0.095	0.179	0.088	−0.013	0.107
ln (Latitude), 0–180	0.352 *	0.023	0.115 *	0.012	−0.003	0.018	0.008	0.021
ln (Longitude), 0–360	0.007 *	0.002	−0.031 *	0.002	−0.029 *	0.002	−0.001	0.002
Sea surface temperature, °C	0.002 *	0.0004	0.001 *	0.0003	0.0001	0.001	−0.001 *	0.0004
Number of grids	5714		6160		6007		5965	
Dependent variable:	Meridional velocities, m/s							
	Quarter 1		Quarter 2		Quarter 3		Quarter 4	
Explanatory variables:	Coefficient	SE	Coefficient	SE	Coefficient	SE	Coefficient	SE
Constant	0.747	0.080	0.254	0.065	0.013	0.052	0.379	0.072
ln (Latitude), 0–180	−0.143 *	0.016	−0.060 *	0.013	−0.009	0.010	−0.076 *	0.014
ln (Longitude), 0–360	−0.010 *	0.002	0.009 *	0.001	0.007 *	0.001	−0.002	0.002
Sea surface temperature, °C	−0.001 *	0.0003	−0.0002	0.0002	−0.0001	0.0002	0.0003	0.0003
Number of grids	5716		6161		6010		5968	
Dependent variable:	Eddy kinetic energy [4], m^2/s^2							
	Quarter 1		Quarter 2		Quarter 3		Quarter 4	
Explanatory variables:	Coefficient	SE	Coefficient	SE	Coefficient	SE	Coefficient	SE
Constant	0.163	0.043	0.381	0.049	0.583	0.043	−0.138	0.199
ln (Latitude), 0–180	−0.027 *	0.008	−0.075 *	0.010	−0.109 *	0.009	0.028	0.039
ln (Longitude), 0–360	−0.006 *	0.001	−0.001	0.001	−0.007 *	0.001	−0.005 *	0.001
Sea surface temperature, °C	0.001 *	0.0002	0.0002 *	0.0001	−0.0001	0.0002	0.002 *	0.001
Number of grids	5714		6160		6007		5965	

[1] Slope coefficients and standard errors are reported using 20 quarterly observations on 1 × 1 degree grids for ocean surface currents zonal and meridional velocities and eddy kinetic energy in the Northern hemisphere. [2] Coefficients of the dummy variables for the years 2002–2019 are suppressed for brevity. [3] Sea surface temperatures were assumed to be correlated with the random effects for grids. [4] Eddy kinetic energy was the sum of the squared zonal and meridional velocities. * $p < 0.05$.

Table 8. Efficient estimates of static random effects models using quarterly data for 2000–2019 for 1 × 1 degree grids on zonal and meridional ocean surface current velocities and eddy kinetic energy in the Southern hemisphere explained by geodesic variables, time indicators for the years, and sea surface temperatures [1,2,3].

Dependent Variable:	**Zonal Velocities, m/s**							
	Quarter 1		**Quarter 2**		**Quarter 3**		**Quarter 4**	
Explanatory variables:	Coefficient	SE	Coefficient	SE	Coefficient	SE	Coefficient	SE
Constant	0.292	0.019	0.414	0.020	0.766	0.022	0.366	0.026
ln (Latitude), 0–180	−0.058 *	0.006	−0.090 *	0.006	−0.182 *	0.006	−0.072 *	0.007
ln (Longitude), 0–360	−0.006 *	0.001	−0.005 *	0.001	−0.007 *	0.001	−0.006 *	0.001
Sea surface temperature, °C	−0.001 *	0.0002	−0.001 *	0.0002	−0.0002	0.0002	−0.002 *	0.0002
Number of grids	17,240		16,879		15,159		15,456	
Dependent variable:	Meridional velocities, m/s							
	Quarter 1		Quarter 2		Quarter 3		Quarter 4	
Explanatory variables:	Coefficient	SE	Coefficient	SE	Coefficient	SE	Coefficient	SE
Constant	0.018	0.013	0.110	0.014	0.267	0.019	0.045	0.020
ln (Latitude), 0–180	−0.003	0.004	−0.029 *	0.004	−0.070 *	0.001	−0.008	0.006
ln (Longitude), 0–360	0.003 *	0.001	0.003 *	0.001	0.001 *	0.006	0.002 *	0.001
Sea surface temperature, °C	−0.001 *	0.0002	−0.001 *	0.0001	0.0004	0.0002	−0.001 *	0.0002
Number of grids	17,241		16,881		15,161		15,458	
Dependent variable:	Eddy kinetic energy [4], m^2/s^2							
	Quarter 1		Quarter 2		Quarter 3		Quarter 4	
Explanatory variables:	Coefficient	SE	Coefficient	SE	Coefficient	SE	Coefficient	SE
Constant	−0.044	0.0001	−0.031	0.009	−0.001	0.010	−0.097	0.010
ln (Latitude), 0–180	0.027 *	0.002	0.021 *	0.003	0.013 *	0.003	0.042 *	0.003
ln (Longitude), 0–360	−0.007 *	0.0002	−0.006 *	0.0003	−0.006 *	0.001	−0.007 *	0.001
Sea surface temperature, °C	−0.001 *	0.0002	−0.0002 *	0.0001	−0.0002 *	0.0001	−0.001 *	0.0001
Number of grids	17,240		16,879		15,159		15,456	

[1] Slope coefficients and standard errors are reported using 20 quarterly observations on 1 × 1 degree grids for ocean surface currents zonal and meridional velocities and eddy kinetic energy in the Southern hemisphere. [2] Coefficients of the dummy variables for the years 2002–2019 are suppressed for brevity. [3] Sea surface temperatures were assumed to be correlated with the random effects for grids. [4] Eddy kinetic energy was the sum of the squared zonal and meridional velocities. * $p < 0.05$.

8. Discussion and Conclusions

This paper analyzed remote sensing data during 2000–2019 for the sea surface temperatures, sea ice concentrations, and zonal and meridional velocities of ocean surface currents in the Northern and Southern hemispheres. Methodological issues such as processing of satellite signals using nonlinear techniques and their implications for the specification of empirical models were addressed. Moreover, the interdependence between climate indicators was embodied in the models, and feedback effects often discussed in the climate literature were rigorously investigated using quarterly longitudinal data for the 1×1 degree grids.

First, the estimated coefficients of indicators variables for years in the models for quarterly sea surface temperatures in Table 3 showed significant increases in the Northern hemisphere. By contrast, cyclical patterns were apparent in the Southern hemisphere in Table 4. Higher emissions of greenhouse gases and greater dumping of pollutants into the oceans from industrial and agricultural activities in the Northern hemisphere were likely to underlie the steady increases. Second, the sea ice concentrations in the previous quarter were negatively associated with sea surface temperatures in both hemispheres thereby indicating the presence of feedback loops. The elasticities of the sea surface temperatures with respect to previous sea ice concentrations from static models for Northern hemisphere for the quarters were -0.075, -0.075, -0.046, and -0.049, respectively. The corresponding elasticities for Southern hemisphere were -0.026, -0.019, -0.048, and -0.058, respectively. Thus, a 50 percent decrease in sea ice concentrations in Northern and Southern hemispheres would predict 3.10 and 1.89 percent increases in sea surface temperatures, respectively. These elasticities were slightly larger than the elasticities of approximately 0.04 of ambient temperatures with respect to carbon dioxide concentrations [7]. Because the declines in sea ice concentrations have serious repercussions for the Earth's radiation budget, such issues merit greater emphasis in policy discussions. The estimated elasticities can also be utilized for making climate projections based on the comprehensive analyses of the longitudinal remote sensing data.

Third, there were steady declines in sea ice concentrations in the Northern hemisphere reflected in the negative coefficients of indicator variables for the years in Table 5. As for the sea surface temperatures, greater cyclical patterns were apparent in the Southern hemisphere, presumably due to the capacity of the vast southern oceans to gradually absorb heat emitted from the Northern hemisphere. The elasticities of sea ice concentrations with respect to sea surface temperatures in the Northern hemisphere for the quarters were -2.23, -1.83, -1.22 and -0.86, respectively. The corresponding estimates for the Southern hemisphere were -3.24, -2.66, -2.94, and -3.00, respectively. The large magnitudes of the elasticities imply proportionately greater declines in sea ice concentrations with increases in sea surface temperatures. For example, a 10 percent increase in the sea surface temperatures would predict 15.4 and 29.6 percent declines in sea ice concentrations in the Northern and Southern hemispheres, respectively. While the magnitudes of the elasticities might have been influenced by interpolations used for processing the satellite signals and the confidence intervals may be wide, the dynamics of sea ice concentrations also depends on the ocean surface and deep-ocean currents. Because these variables can affect the Earth's radiation budget, broader policies should seek to prevent increases in both the ambient and sea surface temperatures.

Fourth, the models for the zonal and meridional velocities of ocean surface currents did not exhibit clear trends for the 1×1 degree grids in Northern and Southern hemispheres. Moreover, internal variations in the velocities were high and were likely to be affected by eddies and the interactions with deep-ocean currents; such variables cannot be easily approximated in practical situations [37]. However, combining the squared values for the two velocities as the eddy kinetic energy led to significant improvements in model adequacy. In particular, the sea surface temperatures were generally significantly and positively associated with eddy kinetic energy in the Northern hemisphere, whereas they were significantly negatively associated in Southern hemisphere. Such issues need to be explored in future research partly due to the somewhat different results for the separate

models estimated for the squared zonal and meridional velocities. Moreover, velocity changes in the Atlantic Meridional Overturning Circulation may have major impacts for global climate patterns and could decrease the ambient temperatures in Europe by up to 10 degrees centigrade [47]. It is important to recognize the possibly asymmetric consequences of higher temperatures for different continents. For example, climate in certain Asian and African countries may become intolerably warm so that the higher sea levels and population growth, together with reduced biodiversity and agricultural productivity due to coastal flooding, could force mass migration to higher grounds [48,49].

Finally, the empirical results underscored the importance of jointly formulating models for the sea surface temperatures, sea ice concentrations, and ocean surface current velocities. The empirical findings such as the large elasticities of sea ice concentrations with respect to sea surface temperatures imply that higher temperatures are likely to rapidly reduce the concentrations of sea ice and thicknesses of polar ice sheets and accelerate the Earth's heating rate [50]. In addition, aerosols from pollution can reduce glacier thicknesses [15,51,52] thereby threatening potable water supplies for many countries. This may also be true for water vapor levels [53] though grid-level longitudinal data were not available. The present climate policy emphasis on containing increases in average ambient temperatures to below 1.5 degrees centigrade [2] seems a minimal target that is unlikely to be met in the current political and economic environments. However, future climatic upheavals may force drastic policy changes. Notwithstanding the uncertainties in the changes in ocean surface current velocities, global sustainability will be enhanced by reductions in greenhouse gas emissions, increases in renewable energy generation, better waste management practices, and reductions in the dumping of industrial and agricultural pollutants into rivers and oceans.

Author Contributions: Conceptualization, methodology, econometric modelling, and writing, A.B.; data downloading and processing, descriptive statistics, and figures, J.A.E. All authors have read and agreed to the published version of the manuscript.

Funding: This research received no external funding.

Institutional Review Board Statement: Not applicable.

Informed Consent Statement: Not applicable.

Data Availability Statement: All data analyzed in the manuscript are available from Copernicus (www.copernicus.eu/en, accessed on 8 October 2022) and Jet Propulsion Labs (https://www.jpl.nasa.gov/, accessed on 8 October 2022).

Acknowledgments: While retaining the responsibility for the analyses, the authors thank Xiayun Tan for her help. Thanks are also due to the two reviewers for several helpful comments.

Conflicts of Interest: The authors declare no conflict of interest.

References

1. Arrhenius, S., XXXI. On the influence of carbonic acid in the air upon the temperature of the ground. *Lond. Edinb. Dublin Philos. Mag. J. Sci.* **1896**, *41*, 237–276. [CrossRef]
2. Intergovernmental Panel on Climate Change (IPCC). Fifth Assessment Report, Working Group III, Summary for Policymakers. 2014. Available online: http://www.ipcc.ch/report/ar5/wg3/ (accessed on 27 October 2018).
3. United Nations. United Nations Climate Change Conference 26. 2021. Available online: https://unfccc.int/cop26 (accessed on 28 November 2021).
4. World Data Centre for Greenhouse Gases. Data Archive. 2021. Available online: https://gaw.kishou.go.jp/ (accessed on 10 August 2020).
5. The Intergovernmental Panel on Climate Change Special Report on the Ocean and Cryosphere in a Changing Climate. Available online: https://www.ipcc.ch/srocc/ (accessed on 10 December 2020).
6. Heimann, M.; Reichstein, M. Terrestrial ecosystem carbon dynamics and climate feedbacks. *Nature* **2008**, *451*, 289–292. [CrossRef] [PubMed]
7. Bhargava, A. Econometric modelling of carbon dioxide emissions and concentrations, ambient temperatures and ocean deoxygenation. *J. R. Stat. Soc. Ser. A Stat. Soc.* **2021**, *185*, 178–201. [CrossRef]

8. Keeling, R.F.; Körtzinger, A.; Gruber, N. Ocean Deoxygenation in a Warming World. *Annu. Rev. Mar. Sci.* **2010**, *2*, 199–229. [CrossRef] [PubMed]
9. Rabalais, N.N.; Turner, R.E.; Díaz, R.J.; Justić, D. Global change and eutrophication of coastal waters. *ICES J. Mar. Sci.* **2009**, *66*, 1528–1537. [CrossRef]
10. Gonzalez-Rivas, D.A.; Tapia-Silva, F.O.; Bustillos-Guzman, J.J.; Revollo-Fernandez, D.A.; Beltran-Morales, L.F.; Lluch-Cota, D.B.; Ortega-Rubio, A. Estimating nitrogen runoff from agriculture to coastal zones by a rapid GIS and remote sensing-based method for a case study from irrigation district Rio Mayo, Gulf of California, Mexico. *Front. Mar. Sci.* **2020**, *7*, 316. [CrossRef]
11. Pucino, M.; Boucher, J.; Bouchet, A.; Paruta, P.; Zgola, M. *Plastic Pollution Hotspotting and Shaping Action: Regional Results from Eastern and Southern Africa, the Mediterranean, and Southeast Asia*; International Union for the Conservation of Nature: Gland, Switzerland, 2020.
12. Timco, G.; Frederking, R. A review of sea ice density. *Cold Reg. Sci. Technol.* **1996**, *24*, 1–6. [CrossRef]
13. Lavers, J.L.; Rivers-Auty, J.; Bond, A.L. Plastic debris increases circadian temperature extremes in beach sediments. *J. Hazard. Mater.* **2021**, *416*, 126140. [CrossRef]
14. Stroeve, J.; Notz, D. Changing state of Arctic sea ice across all seasons. *Environ. Res. Lett.* **2018**, *13*, 103001. [CrossRef]
15. Wadham, J.L.; Hawkings, J.R.; Tarasov, L.; Gergiore, L.J.; Spencer, R.G.M.; Gutjahr, M.; Ridgwell, A.; Kohfeld, K.E. Ice sheets matter for the global carbon cycle. *Nat. Commun.* **2019**, *10*, 3567. [CrossRef]
16. Liu, W.; Fedorov, A.; Sévellec, F. The Mechanisms of the Atlantic Meridional Overturning Circulation Slowdown Induced by Arctic Sea Ice Decline. *J. Clim.* **2019**, *32*, 977–996. [CrossRef]
17. Caesar, L.; McCarthy, G.D.; Thornalley, D.J.R.; Cahill, N.; Rahmstorf, S. Current Atlantic Meridional Overturning Circulation weakest in last millennium. *Nat. Geosci.* **2021**, *14*, 118–120. [CrossRef]
18. EUMETSAT. Ocean and Sea Ice Satellite Application Facility, Global sea ice concentration climate data record 1979-2015 (v2.0, 2017), OSI-450. Copernicus Climate Change Service Climate Data Store. Available online: https://cds.climate.copernicus.eu/cdsapp#!/dataset/satellite-sea-ice-concentration (accessed on 19 August 2020).
19. Merchant, C.J.; Embury, O.; Bulgin, C.E.; Block, T.; Corlett, G.K.; Fiedler, E.; Good, S.A.; Mittaz, J.; Rayner, N.A.; Berry, D.; et al. Satellite-based time-series of sea-surface temperature since 1981 for climate applications. *Sci. Data* **2019**, *6*, 223. [CrossRef]
20. Esr OSCAR Third Degree Resolution Ocean Surface Currents. Available online: https://podaac.jpl.nasa.gov/dataset/OSCAR_L4_OC_third-deg (accessed on 10 August 2020).
21. Wiener, N. *Extrapolation, Interpolation, and Smoothing of Stationary Time Series*; John Wiley & Sons: New York, NY, USA, 1949.
22. Kalman, R.E. A New Approach to Linear Filtering and Prediction Problems. *J. Basic Eng.* **1960**, *82*, 35–45. [CrossRef]
23. Meier, W.N.; The National Center for Atmospheric Research (NCAR) Staff. (Eds). The Climate Data Guide: Sea Ice Concentration: NOAA/NSIDC Climate Data Record. 2014. Available online: https://climatedataguide.ucar.edu/climate-data/sea-ice-concentration-noaansidc-climate-data-record (accessed on 28 November 2021).
24. Ricker, R.; Hendricks, S.; Perovich, D.K.; Helm, V.; Gerdes, R. Impact of snow accumulation on CryoSat-2 range retrievals over Arctic sea ice: An observational approach with buoy data. *Geophys. Res. Lett.* **2015**, *42*, 4447–4455. [CrossRef]
25. Dohan, K. Ocean surface currents from satellite data. *J. Geophys. Res. Oceans* **2017**, *122*, 2647–2651. [CrossRef]
26. Röhrs, J.; Sutherland, G.; Jeans, G.; Bedington, M.; Sperrevik, A.K.; Dagestad, K.-F.; Gusdal, Y.; Mauritzen, C.; Dale, A.; LaCasce, J.H. Surface currents in operational oceanography: Key applications, mechanisms, and methods. *J. Oper. Oceanogr.* **2021**, 1–29. [CrossRef]
27. Lumpkin, R.; Johnson, G.C. Global ocean surface velocities from drifters: Mean, variance, El Niño-Southern Oscillation response, and seasonal cycle. *J. Geophys. Res. Oceans* **2013**, *118*, 2992–3006. [CrossRef]
28. Sykulski, A.M.; Olhede, S.C.; Lilly, J.M.; Danioux, E. Lagrangian time series models for ocean surface drifter trajectories. *J. R. Stat. Soc. Ser. C Appl. Stat.* **2015**, *65*, 29–50. [CrossRef]
29. Timmermans, M.; Marshall, J. Understanding Arctic Ocean Circulation: A Review of Ocean Dynamics in a Changing Climate. *J. Geophys. Res. Oceans* **2020**, *125*. [CrossRef]
30. Kang, D.; Curchitser, E.N. On the Evaluation of Seasonal Variability of the Ocean Kinetic Energy. *J. Phys. Oceanogr.* **2017**, *47*, 1675–1683. [CrossRef]
31. Martínez-Moreno, J.; Hogg, A.M.; Kiss, A.E.; Constantinou, N.C.; Morrison, A.K. Kinetic Energy of Eddy-Like Features From Sea Surface Altimetry. *J. Adv. Model. Earth Syst.* **2019**, *11*, 3090–3105. [CrossRef]
32. Johnson, E.S.; Bonjean, F.; Lagerloef, G.S.E.; Gunn, J.T.; Mitchum, G.T. Validation and Error Analysis of OSCAR Sea Surface Currents. *J. Atmos. Ocean. Technol.* **2007**, *24*, 688–701. [CrossRef]
33. Rayner, N.A.; Parker, D.E.; Horton, E.B.; Folland, C.K.; Alexander, L.V.; Rowell, D.P.; Kent, E.C.; Kaplan, A. Global analyses of sea surface temperature, sea ice, and night marine air temperature since the late nineteenth century. *J. Geophys. Res.* **2003**, *108*, 4407. [CrossRef]
34. Bonjean, F.; Lagerloef, G.S. Diagnostic model and analysis of the surface currents in the Tropical Pacific Ocean. *J. Phys. Oceanogr.* **2002**, *32*, 2938–2954. [CrossRef]
35. Reynolds, R.W.; Smith, T.M.; Liu, C.; Chelton, D.B.; Casey, K.S.; Schlax, M.G. Daily High-Resolution-Blended Analyses for Sea Surface Temperature. *J. Clim.* **2007**, *20*, 5473–5496. [CrossRef]
36. National Centers for Environmental Information. World Ocean Database. 2019. Available online: https://data.nodc.noaa.gov/cgi-bin/iso?id=gov.noaa.nodc:0164586#__sid=js0 (accessed on 10 August 2020).

37. Stommel, H. The westward intensification of wind-driven ocean currents. *Trans. Am. Geophys. Union* **1948**, *29*, 202–206. [CrossRef]
38. Wald, A. *Sequential Analysis*; Dover Publications: New York, NY, USA, 1947.
39. Bhargava, A.; Sargan, J.D. Estimating Dynamic Random Effects Models from Panel Data Covering Short Time Periods. *Econometrica* **1983**, *51*, 1635. [CrossRef]
40. Numerical Algorithm Group. *Numerical Algorithm Group Library. Mark 13*; Oxford University: Oxford, UK, 1990.
41. Bhargava, A. Identification and Panel Data Models with Endogenous Regressors. *Rev. Econ. Stud.* **1991**, *58*, 129–140. [CrossRef]
42. Mann, H.B.; Wald, A. On the Statistical Treatment of Linear Stochastic Difference Equations. *Econometrica* **1943**, *11*, 173–220. [CrossRef]
43. Koopmans, T.; Rubin, H.; Leipnik, R. Measuring the equation systems of dynamic economics. In *Statistical Inference in Dynamic Economic Models*; Koopmans, T.C., Ed.; John Wiley and Sons: New York, NY. USA, 1950; pp. 54–237.
44. Bhargava, A. Wald Tests and Systems of Stochastic Equations. *Int. Econ. Rev.* **1987**, *28*, 789. [CrossRef]
45. Neyman, J.; Scott, E.L. Consistent Estimates Based on Partially Consistent Observations. *Econometrica* **1948**, *16*. [CrossRef]
46. Jensen, M.F.; Nisancioglu, K.H.; Spall, M.A. Large Changes in Sea Ice Triggered by Small Changes in Atlantic Water Temperature. *J. Clim.* **2018**, *31*, 4847–4863. [CrossRef]
47. Weijer, W.; Cheng, W.; Drijfhout, S.; Fedorov, A.; Hu, A.; Jackson, L.; Liu, W.; McDonagh, E.; Mecking, J.; Zhang, J. Stability of the Atlantic Meridional Overturning Circulation: A review and synthesis. *J. Geogr. Res. Ocean.* **2019**, *124*, 5336–5375. [CrossRef]
48. Piguet, E. Environment and migration. International Encyclopedia of Human Geography (2nd edition). *Environ. Migr.* **2020**, *4*, 163–168. [CrossRef]
49. Bhargava, A. Broader frameworks are necessary for climate mitigation policies. *E-Lett. Sci. Mag.* **2021**, *373*, 850–852. [CrossRef]
50. Loeb, N.G.; Johnson, G.C.; Thorsen, T.J.; Lyman, J.M.; Rose, F.G.; Kato, S. Satellite and Ocean Data Reveal Marked Increase in Earth's Heating Rate. *Geophys. Res. Lett.* **2021**, *48*. [CrossRef]
51. GlaThiDa Consortium. *Glacier Thickness Database 3.0.1*; World Glacier Monitoring Service: Zurich, Switzerland, 2019. [CrossRef]
52. Samset, B. *Aerosols and Climate: Oxford Research Encyclopedia*; Climate Science; Oxford University Press: Oxford, UK, 2019.
53. Dessler, A.E.; Schroeberl, M.R.; Wang, T.; Davis, S.M.; Rosenlof, K.H. Stratospheric water vapor feedback. *Proc. Natl. Acad. Sci. USA* **2013**, *110*, 18087–18091. [CrossRef]